Published in final edited form as:
Lasers Surg Med. 2008 September ; 40(7): 461–467. doi:10.1002/lsm.20653.

IN-VIVO NONMELANOMA SKIN CANCER DIAGNOSIS USING RAMAN MICROSPECTROSCOPY

Chad A. Lieber, Ph.D.
CHOC Research Institute, Children's Hospital of Orange County, Orange, CA 92868

Department of Biomedical Engineering, Vanderbilt University, Nashville, TN 37235

Shovan K. Majumder, Ph.D.
Laser Biomedical Applications & Instrumentation Division, Raja Ramanna Center for Advanced Technology, Indore, India

Department of Biomedical Engineering, Vanderbilt University, Nashville, TN 37235

Darrel L. Ellis, M.D.
Division of Dermatology, Vanderbilt University Medical Center, Nashville, TN 37232

D. Dean Billheimer, Ph.D.
Division of Biostatistics, Vanderbilt University Medical Center, Nashville, TN 37232

Biostatistics Shared Resource, Huntsman Cancer Institute, University of Utah, Salt Lake City, UT 84112

Anita Mahadevan-Jansen, Ph.D.
Department of Biomedical Engineering, Vanderbilt University, Nashville, TN 37235

Abstract

Background and Objective—Nonmelanoma skin cancers, including basal cell carcinoma (BCC) and squamous cell carcinoma (SCC), are the most common skin cancers, presenting nearly as many cases as all other cancers combined. The current gold-standard for clinical diagnosis of these lesions is histopathologic examination, an invasive, time-consuming procedure. There is thus considerable interest in developing a real-time, automated, noninvasive tool for nonmelanoma skin cancer diagnosis. In this study, we explored the capability of Raman microspectroscopy to provide differential diagnosis of BCC, SCC, inflamed scar tissue, and normal tissue *in vivo*.

Study Design—Based on the results of previous *in vitro* studies, we developed a portable confocal Raman system with a handheld probe for clinical study. Using this portable system, we measured Raman spectra of 21 suspected nonmelanoma skin cancers in 19 patients with matched normal skin spectra. These spectra were input into nonlinear diagnostic algorithms to predict pathological designation.

Results—All of the BCC (9/9), SCC (4/4), and inflamed scar tissues (8/8) were correctly predicted by the diagnostic algorithm, and 19 out of 21 normal tissues were correctly classified. This translates into a 100% (21/21) sensitivity and 91% (19/21) specificity for abnormality, with a 95% (40/42) overall classification accuracy.

Conclusions—These findings reveal Raman microspectroscopy to be a viable tool for real-time diagnosis and guidance of nonmelanoma skin cancer resection.

Corresponding Author Chad A. Lieber, Ph.D. CHOC Research Institute Children's Hospital of Orange County 455 South Main St. Orange, CA 92868 Ph. 714-516-4257 Fx. 714-516-4318 clieber@choc.org.

Keywords

automated diagnosis; optical spectroscopy; basal cell carcinoma; squamous cell carcinoma; scar tissue

INTRODUCTION

Nonmelanoma skin cancers, including basal cell carcinoma (BCC) and squamous cell carcinoma (SCC), are the most common amongst cancers of the skin, their incidence nearly equal to that of all other cancers combined.(1) Although these cancers are often slow-growing, nonmelanoma skin cancers can cause significant local damage and can metastasize if left untreated. The gold-standard for diagnosis of these lesions is biopsy and subsequent histopathologic correlation. This process is both invasive and time-consuming (~one week at Vanderbilt University Medical Center). Furthermore, therapeutic intervention typically depends on the lesion pathology, extent of proliferation, and patient history. Consequently, several clinical visits are often required for accurate diagnosis and curative therapy. There is thus considerable interest in the development of an automated, non-invasive, real-time diagnostic technique for skin lesions.

Raman spectroscopy is an optical technique that probes the vibrational activity of chemical bonds, thus each molecule has a spectral signature characteristic of its modes of vibration. These spectral signatures can be used to identify unknown substances in a sample, or to differentiate samples according to their chemical constituency. Raman spectroscopy is ideal for *in vivo* tissue diagnosis, as it is non-destructive, does not require external dyes, and can be applied via fiber-based or conventional optics-based instrumentation with clinically feasible measurement times. Furthermore, this technique can be applied in a confocal arrangement to allow spatially resolved Raman spectra for margin delineation. Raman spectroscopy has been used to successfully differentiate a variety of tissues in numerous organ sites, but skin provides an ideal measurement site for this optical technique, due to its obvious accessibility.

Several groups have utilized Raman spectroscopy for the study of skin biochemistry. Caspers *et al*.(2–5) have characterized the molecular composition and hydration gradients of skin both *in vitro* and *in vivo* using confocal Raman spectroscopy. Natural variations in skin composition and hydration have also been studied,(6) and spectra were found to be reproducible between and within patients, with minor variations attributed to skin hydration state. The conformational structures of skin proteins, water, and lipids were analyzed *in vitro* using Raman spectroscopy,(7) and the degree of preservation of these structures was assessed in mummified skin.(8)

Skin disease has also been investigated using the Raman technique. Raman spectral intensities of carotenoids in human skin have been found to be increased in actinic keratosis and BCC as opposed to site-matched normal skin.(9) Edwards *et al*.(10) showed variations in Raman spectra between normal skin and hyperkeratotic lesion samples to be related to lipid concentration. Gniadecka *et al*.(11) found lipid and protein structures to differ between BCC and normal skin biopsies, and were able to use the respective Raman intensities to achieve a complete separation between these tissue types. Simple analysis of Confocal Raman spectra obtained from various skin depths by Choi *et al.* showed a 95% separation between normal and BCC.(12) Confocal Raman maps of BCC sections have also been shown to accurately identify tumor margins, with 100% sensitivity and 93% specificity.(13) The same group has also demonstrated the capabilities of high wavenumber Raman bands (2800 to 3125 cm^{-1}) to discriminate BCC from perilesional tissue.(14) All of these reports show that Raman spectroscopy can provide diagnostically useful information about human skin.

However, none of these groups have explored the ability of Raman spectroscopy to provide diagnosis of nonmelanoma skin cancers (BCC and SCC) and inflamed scar tissue *in vivo*. This distinction is especially important for the dermatologist to recognize tumor areas from scarred areas of previous biopsy or surgical resection. Additionally, there has been little reported on the use of a depth-resolved Raman approach for *in vivo* skin disease diagnosis. Depth resolution (confocality) minimizes the spectral measurement volume, thereby reducing spectral contributions from surrounding tissue. Thus, the goal of this study is to evaluate the potential of Raman microspectroscopy to provide clinical diagnosis of nonmelanoma skin cancer (BCC and SCC), normal, and scarred skin tissue. In a previous *in vitro* pilot study of 39 skin samples, a significant difference between melanoma, BCC, SCC, and normal skin Raman spectra was found.(15) Based on these results, a handheld confocal Raman microscope was developed for clinical application.(16) Using this portable system, depth-resolved Raman spectra were measured *in vivo* from a number of suspected BCC, SCC and adjacent normal skin areas. Diagnostic algorithms were developed to quantitatively assess the ability of Raman spectroscopy to differentiate between the pathologies, including BCC, SCC, inflamed scar tissue, and normal skin.

MATERIALS AND METHODS

Raman Instrumentation

Raman spectra were collected with a handheld Raman microspectrometer developed specifically for portable clinical application, illustrated in figure 1, described in detail elsewhere.(16) In short, the system utilizes an 825 nm external-cavity diode laser that is fiber-coupled to the handheld probe, which contains a translatable 20×, 0.35 NA near-infrared-optimized objective (Nachet, France). Axial positioning and sample stabilization are maintained by a fused-silica window in the probe. The collected Raman signal is fiber-coupled from the probe to a holographic spectrograph (Kaiser Optical Systems, Ann Arbor, MI) and a thermo-electrically cooled, back-illuminated, deep-depletion CCD (Roper Scientific, Trenton, NJ).

A targeting reticle with removable collar allows positioning of the handheld probe on the skin surface with a lateral positioning accuracy of 400 μm. Axial resolution of the system is 14 μm, and spectral resolution of the system is <7 cm^{-1}.

Measurement Protocol

Raman spectra were measured from 19 patients as part of this study, approved by the Vanderbilt University Medical Center Institutional Review Board (IRB). A total of 21 lesions were measured, along with adjacent normal skin for each lesion, for a total of 42 spectra. Informed consent was obtained from each patient prior to the study. Measurements were made in patients with known (by previous diagnostic procedures) or suspected nonmelanoma skin cancers prior to surgical excision. A Raman spectrum was obtained from the interior of the presumed tumor margin, as determined by the surgeon, and one Raman spectrum was obtained from nearby non-affected skin after both sites had been cleaned by an alcohol swab. The non-affected (perilesional normal) measurements were made at a nominal distance of 1 cm from the presumed tumor margin. All spectra were measured at a depth 40 μm below the skin surface using 30 second integration and 40 mW laser power, as that depth showed high classification accuracy in a previous *in vitro* study.(15) A spot of indelible ink was used to identify the spectral measurement location within the margin, and this location was punch-biopsied for histopathologic correlation. The punch biopsies were fixed in 10% formalin solution, sectioned and mounted on microscope slides, and stained in hematoxylin and eosin (H&E) for histopathologic correlation. Morphometric measurements were made digitally via the microscope software during the histopathologic correlation, to determine the depth of the lesions from the skin surface. In five of the pathologic samples, erosion of the stratum corneum and/or tearing of the tissue during processing prohibited these measurements.

Spectral Processing

Prior to the spectral acquisition in each patient, the spectral dispersion of the detection system was calibrated using the atomic emission lines of a neon-argon lamp, and Raman shift calibration was performed using naphthalene and acetaminophen standards. To allow direct comparison of the spectra, wavenumber binning to one-half the spectral resolution was performed. High frequency spectral noise was removed with a 2nd order Savitzky-Golay filter (17) with a window size of two-times the spectral resolution, and broadband tissue autofluorescence was subtracted using an automated polynomial fitting technique.(18)

Data Analysis

Because the diagnostic algorithms used for spectral classification mathematically transform the spectra into new feature-space, it is not possible to determine the diagnostically relevant features in wavenumber space. Thus, an initial analysis was performed to qualitatively determine the statistically significant differences between the tissue spectra. Though these results were not used in the diagnostic algorithms, they allowed exploration of the responsible mechanisms for comparison to previous studies.

To qualitatively identify spectral differences between the pathologic and normal spectra, standard error confidence intervals were utilized. The variance of the intensity at each wavenumber was first calculated for each pathological spectra set. The composite variance (S^2) of the lesions was then calculated at each wavenumber as:

$$S_{lesions}^2(\lambda) = \frac{\sum_i s(\lambda)_i^2 (df)_i}{\sum_i df_i}$$

where s^2 is the variance of the intensity at each wavenumber λ for each lesion pathology *i*, and *df* corresponds to the degrees of freedom for each pathology (=number of tissue specimens-1). The standard error (*SE*) of the mean difference between lesion spectra and normal skin spectra was then calculated at each wavenumber as:

$$SE_{difference}(\lambda) = \sqrt{\frac{S_{normal}^2(\lambda)}{n_{normal}} + \frac{S_{lesions}^2(\lambda)}{n_{lesions}}}$$

where S^2 is the variance of the intensities at each wavenumber of each tissue type (normal or composite of lesions), and *n* is the number of tissue specimens included in each mean. The standard error was multiplied by appropriate *t* values (based on total degrees of freedom and 99% confidence level) to produce a confidence interval. Difference spectra for the abnormal pathologies with respect to the normal were overlaid on these confidence intervals to qualitatively identify statistically significant spectral differences.

The quantitative analysis of the spectra involved two steps: extraction of diagnostically relevant spectral information through maximum representation and discrimination feature

(MRDF), and classification via sparse multinomial logistic regression (SMLR). These techniques have been described in detail elsewhere,(19,20) and were the same processing methods employed in our previous *in vitro* study.(15) In brief, MRDF is an iterative procedure that aims to find a set of nonlinear transformations on the input data that optimally discriminate between the different classes in a reduced dimensionality space. SMLR separates a set of labeled input data into its constituent classes by predicting the posterior probabilities of their class-membership.

The inputs to these algorithms were the processed spectra after normalization according to the scheme described by Talukder and Casasent.(20) All analyses were performed using full (leave-one-out) cross validation. Each spectrum was classified to the predicted class membership (pathology) with the highest posterior probability.

RESULTS

The mean spectra of all tissue pathologies studied are shown in figure 2, and are similar to those reported in other Raman spectroscopic studies of human skin.(4,5,13) Several qualitative differences can be observed between the spectra at 920–940 cm^{-1}, likely corresponding to C—C stretching in the collagen backbone, 1000–1010 cm^{-1} (phenylalanine, keratin), 1060–1070 cm^{-1} (lipids), 1250–1330 cm^{-1} (protein amide III, lipids), the CH_2 deformation mode of lipids and proteins at 1445 cm^{-1}, and the 1650 cm^{-1} peak attributed to protein amide I and C=C stretch in lipids.(5,10,13,21)

Figure 3 shows the mean difference spectra of each pathology minus their matched normals, as well as the 99% confidence intervals of their standard errors (gray bands) using 38 degrees of freedom (d.o.f.=number of spectral measurements-number of pathologic classes) and 0.01 significance level (α); t value=2.71. A number of significantly different Raman bands are observed for each pathology. Inflamed scar tissue shows significant peaks at 768–782, 789–814, 1178–1188, 1300–1356, and 1643–1671 cm^{-1}, BCC's at 758–772, 807–821, and 1542–1556 cm^{-1}, and SCC's at 551–562, 569–590, 698–716, 1062–1111, 1132–1157, 1412–1423, 1475–1496, 1633–1643, and 1671–1689 cm^{-1}. These regions are listed in table I along with likely band assignments, where possible.

The posterior probabilities, as determined by the MRDF and SMLR algorithms, are shown in figure 4, as grouped by histopathology. This figure shows that only two samples are misclassified, normal samples with the highest posterior probability of SCC. It is also evident that the scar and BCC spectra are largely well separated from the other tissues, while the SCC tissues generally show a moderate probability for normal tissue. In total, all of the abnormal spectra are correctly classified, including all 8 inflamed scar tissues, 9 BCC, and 4 SCC, while 19 of the 21 normals are classified as normal. These numbers translate into a 100% (21/21) sensitivity and 91% (19/21) specificity for abnormality, with a 95% (40/42) overall classification accuracy.

Morphometric measurements of the depth of the proximal tumor margin from the skin surface was possible in 6 of the 9 BCC, and 3 of the 4 SCC. The remaining nonmelanoma sections and several of the scar tissue sections exhibited an erosion of the stratum corneum that prohibited such measurement. The measured depths of the tumor margins were 49, 69, 89, 169, 223, 234, 593, 888, and 961 μm from the surface.

DISCUSSION

Several of these differences reveal that the pathologic spectra can largely be separated by protein- and lipid-related Raman activity. The origins of the peaks in the 807–814 cm^{-1} region remain to be elucidated, but may possibly be due to lipid content or possibly an artifact of silica signal from the measurement optics. Lipid loss in the abnormal tissues is a likely explanation for the Raman peaks in the 1069–1073 cm^{-1} range, as described by Edwards *et al*.(10) The 1321–1325 cm^{-1} range also contains lipid Raman peaks,(10) as well as a shoulder of the 1335 cm^{-1} collagen/DNA peak.(21) Tryptophan produces a Raman peak at 1548 cm^{-1},(21) and is a likely contributor to the differences in the region of 1542–1556 cm^{-1}.

Our results show that the Raman spectra classify the inflammation and BCC with high probability. The two classification errors result when presumed normal skin tissue is classified as SCC. It is also evident that the SCC samples, while classified as such, show reasonable probabilities of normal tissue. Because histopathologic correlation was not available from the perilesional measurement sites, it is possible that these sites contained hyperplastic cells. Another possibility for the confusion between normal and SCC may derive from the cellular nature of the tissues: SCC is derived from keratinocytes, which are the predominant cell in the epidermis of normal skin. While many reports have demonstrated various optical approaches for classification of BCC versus normal, or nonmelanoma (pooled BCC and SCC) versus normal, there is a dearth of studies focused on distinct classification of SCC. Thus, continued patient recruitment and future reports from this and other groups will be necessary to elucidate this matter.

The single 40 μm measurement depth was selected for two reasons: to limit the clinical time required by multiple acquisitions at various depths, and because our previous studies of *ex vivo* skin lesions showed this depth to provide high diagnostic accuracy. In this study, the morphometric measurements of the stained tissue sections showed that the proximal tumor margins in all of the samples measured were located at a depth greater than the ~47 μm Raman measurement depth (40 μm +/− ~7 μm axial resolution). However, as demonstrated, the Raman spectra obtained from this depth are still capable of classifying the tumor spectra with high accuracy. One possible hypothesis for the diagnostic success despite out-of-volume measurements is that the high degree of scattering and refractive mismatches encountered *in vivo* cause broadening of the tightly focused light impingent on the tissue, thus the actual measurement volume encountered *in vivo* was actually larger than that determined in air.(22,23) While this could explain those measurements in which the lesion depth was within tens of microns of the theoretical 40 μm collection depth, it is unlikely to explain the diagnostic success in lesions which were up to several hundred μm below the theoretical collection depth. An alternate hypothesis is that the Raman spectra were detecting malignancy-associated changes (MAC's) in the morphologically normal tissue surrounding the lesions. MAC's were hypothesized roughly 50 years ago on the premise that normal tissue is biochemically altered by chemical signaling from adjacent tumor cells.(24) Recent work has shown that MAC's can be detected via precise morphometric measurements of nuclear size and distribution in light-microscopy images of stained tissue sections or cell smears.(25–28) Though there have been little or no reports focused on their detection using optical spectroscopies, it is presumable that biochemically sensitive techniques such as Raman spectroscopy may be capable of detecting the described changes. This presumption is bolstered by the results of Crow *et al.*, in which Raman spectra were shown to be capable of determining the stage of bladder tumor invasion, (29) implying that such invasion yields distinct biochemical changes in adjacent tissue. Subsequent experiments are currently being developed to further examine whether the molecular specificity of the Raman technique can be used to detect the biochemical malignancy-associated changes which are indiscernible during histopathologic examination.

Because of the classification success despite disparity between Raman measurement location and lesion location, the advisability of a confocal measurement geometry for Raman-based classification of skin lesions is questioned. In a previous *ex-vivo* study of skin lesions, we evaluated the diagnostic capabilities of confocal Raman spectra measured at various depths (from surface to at least 100 μm) as well as integrated spectra from all depths to roughly approximate a non-confocal measurement geometry.(15) The results showed that the integrated spectra produced only slightly more classification error than two of the measured depths, and less than the four other measured depths. However, the integrated spectra were only a rough approximation of the results one would obtain from a non-confocal probe (*i.e.* contact fiber-bundle probe), and a true comparison of confocal versus various non-confocal probe designs for skin cancer detection is warranted. Such a test could directly answer which measurement geometry would be most appropriate for diagnosis of skin lesions.

Though several aforementioned studies have explored the spectral differences between normal skin or actinic keratoses and nonmelanoma skin cancers, it is especially useful to explore the spectral differences between inflamed scar tissue and BCC or SCC. This is evident in hindsight, as the desired pathological spectral measurements were to be made only on suspected (by the dermatologists' examination) BCC and SCC. Yet, upon histopathological examination of the measurement sites, nearly 40% (8 of 21) of these suspected nonmelanoma skin cancers were revealed to be inflamed scar tissue from previous biopsy or surgical excision. Because further surgery would not be needed on an inflamed scar without the presence of the BCC or SCC, it is thus apparent that the clinician could benefit from a noninvasive diagnostic tool of this nature to allow more informed guidance of follow-up procedures. This technique may therefore eventually provide clinicians an automated, rapid, noninvasive tool to streamline both diagnostic and therapeutic skin cancer procedures.

It should be noted that the diagnostic algorithms developed in this study were based on spectra from a limited number of patients assumed to be representative of the entire patient population. The patient selection criteria as well as the limited number of spectra in each pathologic category might influence the classification results obtained in this study. Therefore, further clinical studies in a larger patient population, which are already in progress, will be used to validate the classification estimates presented here.

Acknowledgments

This work was supported by a National Institutes of Health R21 grant (#CA95995). The authors would also like to thank Dr. Hunter Sams and Dr. Thomas Stasko for their assistance in the clinical measurements.

REFERENCES

1. Jemal A, Siegel R, Ward E, Murray T, Xu J, Thun MJ. Cancer Statistics, 2007. CA: A Cancer Journal for Clinicians. 2007; 57(1):43–66. [PubMed: 17237035]
2. Caspers PJ, Lucassen GW, Bruining HA, Puppels GJ. Automated depth-scanning confocal Raman microspectrometer for rapid in vivo determination of water concentration profiles in human skin. J Raman Spectrosc. 2000; 31:813–818.
3. Caspers PJ, Lucassen GW, Carter EA, Bruining HA, Puppels GJ. In vivo confocal Raman microspectroscopy of the skin: Noninvasive determination of molecular concentration profiles. J Invest Dermatol. 2001; 116(3):434–442. [PubMed: 11231318]
4. Caspers PJ, Lucassen GW, Puppels GJ. Combined in vivo confocal Raman spectroscopy and confocal microscopy of human skin. Biophys J. 2003; 85:572–580. [PubMed: 12829511]
5. Caspers PJ, Lucassen GW, Wolthuis R, Bruining HA, Puppels GJ. In vitro and in vivo Raman spectroscopy of human skin. Biospectroscopy. 1998; 4:S31–S39. [PubMed: 9787912]
6. Knudsen L, Johansson CK, Philipsen PA, Gniadecka M, Wulf HC. Natural variations and reproducability of in vivo near-infrared Fourier transform Raman spectroscopy of normal human skin. J Raman Spectrosc. 2002; 33:574–579.

7. Gniadecka M, Nielsen OF, Christensen DH, Wulf HC. Structure of water, proteins, and lipids in intact human skin, hair, and nail. J Invest Dermatol. 1998; 110(4):393–398. [PubMed: 9540981]
8. Peterson S, Faurskov Nielsen O, Christensen DH, Edwards HGM, Farwell DW, David R, Lambert P, Gniadecka M, Wulf HC. Near-infrared Fourier transform Raman spectroscopy of skin samples from the `Tomb of the Two Brothers,' Khnum-Nakht and Nekht-Ankh, XIIth Dynasty Egyptian mummies (ca 2000 BC). J Raman Spectrosc. 2003; 34:375–379.
9. Hata TR, Scholz TA, Ermakov IV, McClane RW, Khachik F, Gellermann W, Pershing LK. Non-invasive raman spectroscopic detection of carotenoids in human skin. J Invest Dermatol. 2000; 115(3):441–448. [PubMed: 10951281]
10. Edwards HGM, Williams AC, Barry BW. Potential applications of FT-Raman spectroscopy for dermatological diagnostics. J Molec Struct. 1995; 347:379–388.
11. Gniadecka M, Wulf HC, Mortensen NN, Nielsen OF, Christensen DH. Diagnosis of basal cell carcinoma by Raman spectroscopy. J Raman Spectrosc. 1997; 28:125–129.
12. Choi J, Choo J, Chung H, Gweon DG, Park J, Kim HJ, Park S, Oh CH. Direct observation of spectral differences between normal and basal cell carcinoma (BCC) tissues using confocal Raman microscopy. Biopolymers. 2005; 77:264–272. [PubMed: 15657894]
13. Nijssen A, Bakker Schut TC, Heule F, Caspers PJ, Hayes DP, Neumann MHA, Puppels GJ. Discriminating basal cell carcinoma from its surrounding tissue by Raman spectroscopy. J Invest Dermatol. 2002; 119:64–69. [PubMed: 12164926]
14. Nijssen A, Maquelin K, Santos LF, Caspers PJ, Schut TCB, den Hollander JC, Neumann MHA, Puppels GJ. Discriminating basal cell carcinoma from perilesional skin using high wave-number Raman spectroscopy. J Biomed Opt. 2007; 12:034004. [PubMed: 17614712]
15. Lieber CA, Majumder SK, Billheimer DD, Ellis DJ, Mahadevan-Jansen A. Raman microspectroscopy for skin cancer detection in-vitro. J Biomed Opt. 2008; 13(2):024013. [PubMed: 18465976]
16. Lieber CA, Mahadevan-Jansen A. Development of a handheld Raman microspectrometer for clinical dermatologic applications. Opt Express. 2007; 15(19):11874–11882. [PubMed: 19547550]
17. Savitzky A, Golay MJE. Smoothing and differentiation of data by simplified least squares procedures. Anal Chem. 1964; 36:1627–1639.
18. Lieber CA, Mahadevan-Jansen A. Automated method for subtraction of fluorescence from biological Raman spectra. Appl Spectrosc. 2003; 57(11):1363–1367. [PubMed: 14658149]
19. Majumder SK, Gebhart S, Johnson MD, Thompson R, Lin WC, Mahadevan-Jansen A. A probability-based spectroscopic diagnostic algorithm for simultaneous discrimination of brain tumor and tumor margins from normal brain tissue. Appl Spectrosc. 2007; 61(5):548–557. [PubMed: 17555625]
20. Talukder A, Casasent D. A genral methodology for simultaneous representation and discrimination of multiple object classes. Opt Eng. 1998; 37(3):904–913.
21. Stone N, Kendall C, Shepherd N, Crow P, Barr H. Near-infrared Raman spectroscopy for the classification of epithelial pre-cancers and cancers. J Raman Spectrosc. 2002; 33:564–573.
22. Everall NJ. Confocal Raman microscopy: why the depth resolution and spatial accuracy can be much worse than you think. Appl Spectrosc. 2000; 54(10):1515–1520.
23. Matousek P, Clark IP, Draper ERC, Morris MD, Goodship AE, Everall N, Towrie M, Finney WF, Parker AW. Subsurface probing in diffusely scattering media using spatially offset Raman spectroscopy. Appl Spectrosc. 2005; 59(4):393–400. [PubMed: 15901323]
24. Nieburgs, HE.; Zak, RG.; Allen, DC.; Reisman, H.; Clardy, T. Systemic cellular changes in material from human and animal tissues in presence of tumors. Transactions of the Seventh Annual Meeting of the International Society of Cytology Council; 1959. p. 137
25. Mairinger T, Mikuz G, Gschwendtner A. Nuclear chromatin texture analysis of nonmalignant tissue can detect adjacent prostatic adenocarcinoma. Prostate. 1999; 41(1):12–19. [PubMed: 10440871]
26. Guillaud M, Cox D, Adler-Storthz K, Malpica A, Staerkel G, Matisic J, Van Niekerk D, Poulin N, Follen M, MacAulay C. Exploratory Analysis of Quantitative Histopathology of Cervical Intraepithelial Neoplasia: Objectivity, Reproducibility, Malignancy-Associated Changes, and Human Papillomavirus. Cytom Part A. 2004; 60:81–89.

27. Susnik B, Worth A, LeRiche J, Palcic B. Malignancy-associated changes in the breast. Changes in chromatin distribution in epithelial cells in normal-appearing tissue adjacent to carcinoma. Anal Quant Cytol. 1995; 17(1):62–68.

28. Macaulay C, Lam S, Payne PW, Leriche JC, Palcic B. Malignancy associated changes in bronchial epithelial cells in biopsy specimens. Anal Quant Cytol. 1995; 17(1):55–61.

29. Crow P, Uff JS, Farmer JA, Wright MP, Stone N. The use of Raman spectroscopy to identify and characterize transitional cell carcinoma in vitro. BJU international. 2004; 93(9):1232–1236. [PubMed: 15180613]

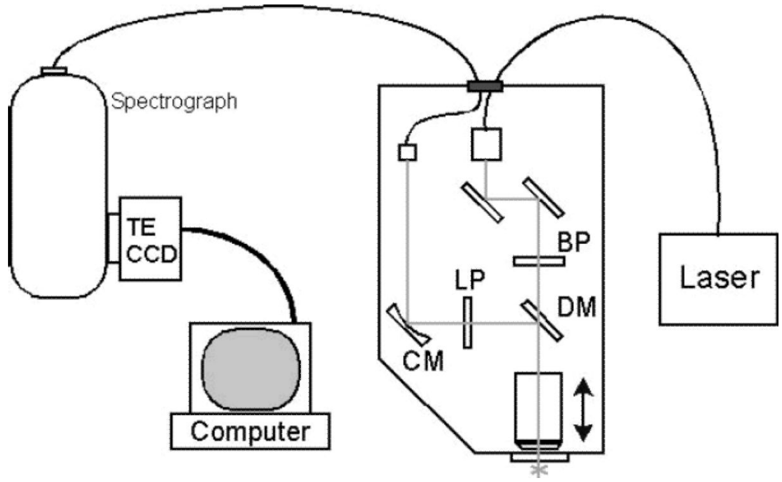

Figure 1.

Schematic of Raman microspectrometer used for *in vivo* skin measurements. Handheld probe is fiber coupled to laser and spectrometer. BP: bandpass filter, DM: dichroic mirror, LP: longpass filter, CM: concave mirror.

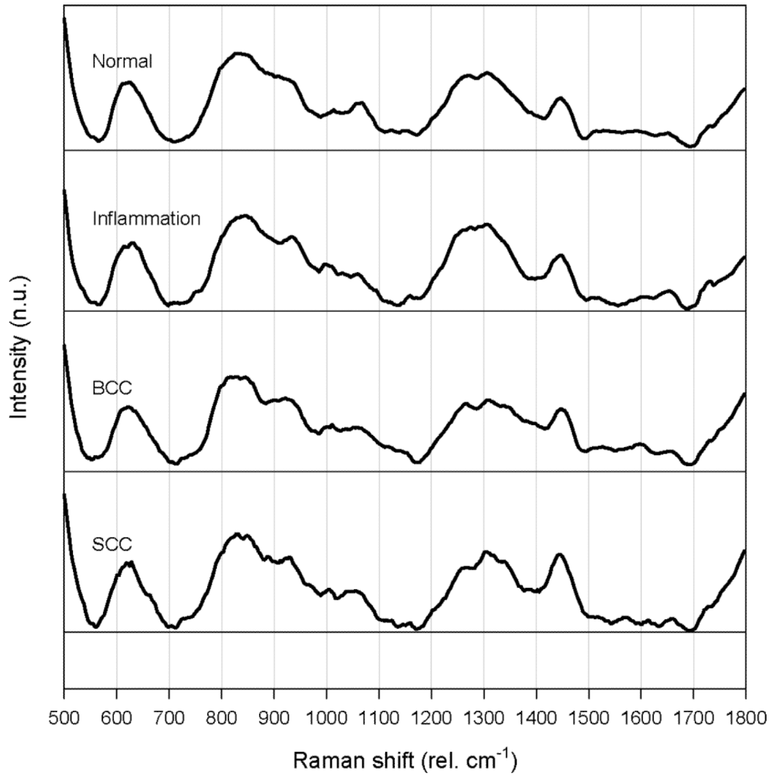

Figure 2.
Mean Raman spectra of skin pathologies studied, normalized to mean intensity for direct comparison.

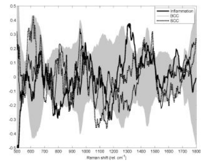

Figure 3.
Statistical differences between the pathologic and normal spectra determined by standard error confidence intervals. Gray bands indicate the 99% confidence intervals of pathologic difference spectra (spectraset minus respective normal).

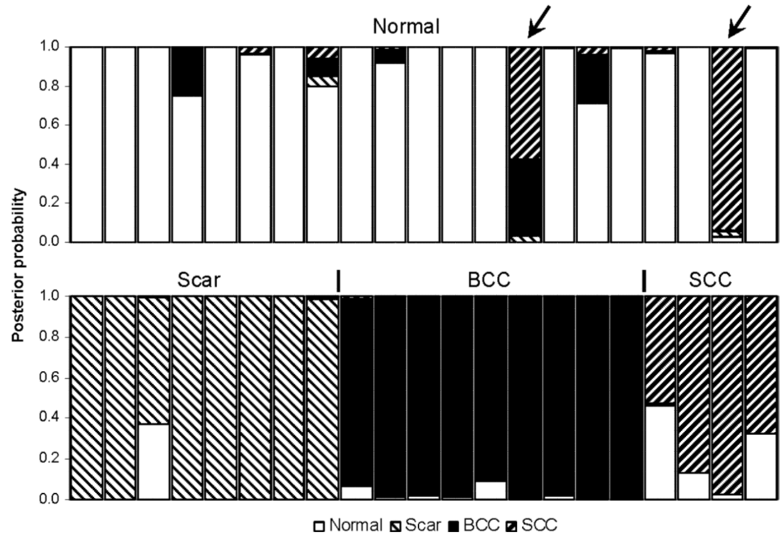

Figure 4.

Posterior probability distributions for all samples studied. Perilesional normal spectra are shown in top figure, and pathologic spectra are shown in lower; labels above each plot correspond to histopathology, while the shading reveals the posterior probability for each pathological classification. Arrows indicate the two misclassified spectra.

TABLE I

Regions of Raman band differences between respective skin lesions and adjacent normal skin (from standard error analysis) with tentative assignments.

Raman Band Region (rel. cm^{-1})				
Inflammation	**BCC**	**SCC**	**Assignment**	**Reference**
		551–562	-	
		569–590	-	
		698–716	phospholipids, nucleotides	(21)
	758–772		tryptophan	(21)
768–782			cytosine/uracil (nucleotides)	(21)
789–814			-	
	807–821		-	
		1062–1111	lipids, proteins	(5,10,13,21)
		1132–1157	lipids, proteins, carotenoids	(5,21)
1178–1188			-	
1300–1356			lipids, collagen, protein amide III, DNA purine bases, phenylalanine	(10,13,21)
		1412–1423	-	
		1475–1496	-	
	1542–1556		tryptophan	(21)
		1633–1643	-	
1643–1671			lipids, protein amide I	(5,10,13,21)
		1671–1689	protein amide III	(5)